Proceedings of the 21st ICSMGE, Vienna, Austria, 14 – 19 June 2026. Pistrol, Adam & Schweiger (eds.)
Published by: ÖGG, Austrian Society for Geomechanics, Salzburg, Austria, ISBN 978-3-9503898-4-5
https://doi.org/10.53243/ICSMGE2026-1723

Morphological characteristics of soil arching and its effect on tunnels

Nidhi Verma, Venkateshwara Reddy K L, Ankit Kumar, Dasaka Satyanarayana Murty
Indian Institute of Technology Bombay, India, 23D285@iitb.ac.in

T. I. George
Virginia Tech, Blacksburg, United States

ABSTRACT: The rapid development of transportation infrastructure requires the construction of underground tunnels. The overburden pressure on tunnels causes the structures to deform, leading to the settlement of the soil above. This, in turn, results in a reorientation of stress in the yielding zone, and the consequence is a reduction in vertical pressure over the deformed shape of a tunnel, a phenomenon known as "soil arching." In existing studies on soil arching and its effects on tunnels, researchers have seldom considered critical aspects, such as tunnel shape, tunnel flexibility, and the depth factor. In this proposed study, a series of finite element analyses are performed to uncover the underlying mechanisms of soil arching mobilization and its morphological characteristics (e.g., the initial arch angle resulting from soil-structure interaction, the thickness of the soil arch, its rise/height, the orientation of principal stresses along the arch, the influence zone, the yielding zone, surface settlements, and the magnitude of force transfer). Notably, the reduction of forces on the critical sections of the tunnel is a significant contribution of this study, offering substantial cost savings in both design and construction.

KEYWORDS: Soil arching, effects on tunnels.

1 INTRODUCTION

Tunnels are a crucial part of modern infrastructure, providing efficient transportation and utilities while navigating difficult geological conditions. Tunnel construction can cause settlements and stress redistributions that affect stability and serviceability, particularly in soft or variable soils. The soil arching effect is the key component of this interaction, transferring load from the excavation onto the adjacent undisturbed ground. The majority of studies ignore important real-world features such as tunnel geometry, lining flexibility, and the amplifying or reducing influence of tunnel depth, even though they provide fundamental descriptions of soil arching. The success of tunnel construction depends heavily on the accuracy of software tools used for analysis and careful planning of the construction steps. This paper emphasizes the importance of precise tunnel analysis by thoroughly validating software predictions with field measurements. It also compares two different construction methods: one where structural load is applied before tunneling, and another where tunneling occurs before applying structural load. The goal is to better understand how software predictions, real-world conditions, and construction sequences interact, ultimately offering valuable insights to improve tunneling techniques. By combining theoretical models, practical measurements, and real-world case studies, this research aims to bridge the gap between software-based tunnel design and actual construction practices, thereby promoting improvements in the reliability and efficiency of tunnel infrastructure development.

1.1 *Soil Arching*

The process where pressure is partially or fully transferred from a deforming soil mass to an adjacent stable or stationary mass is known as soil arching (Karl Terzaghi, 1943). During tunnelling, the redistribution of stresses within the ground occurs when a tunnel is excavated. Normally, the vertical loads from the overlying soil would transfer directly downward, but tunnel construction interrupts this path. As a result, a portion of the load is redirected sideways to more stable ground adjacent to the tunnel opening (Chen et al., 2022).

This phenomenon occurs due to changes in ground support and deformation around the tunnel, along with variations in the soil strength and frictional behaviour. After excavation, the soil directly above the tunnel may settle or experience localized ground loss. However, the surrounding soil forms natural 'arches', shifting much of the load to areas that remain less disturbed (Franza, Marshall and Zhou, 2019). Various studies show distinct zones (N. Loganathan and H. G. Poulos, 1998; Khandouzi and Khosravi, 2023; Song et al., 2023), referred to as the disturbed zone, is directly above the tunnel where settlement is likely to occur. The arching zone, which redirects stress laterally, carries the load to more stable surrounding soil (Lin et al., 2019). The stable zone, beyond the influence of stress changes, remains largely unaffected. This lateral load transfer reduces vertical stress directly above the tunnel crown.

Studies performed by Song et al. (2023) show that the traditional loosening earth pressure theory (Terzaghi) overestimates overburden pressure in sand (by 5%) and underestimates it in clay (by 18%) compared to detailed numerical simulations. The stress transfer (arching) effect is much more pronounced in sandy than in clayey soils, where the arching is weaker and more transient due to slower dissipation of excess pore pressures.

2 NUMERICAL MODELING

2.1 *Case Study*

This numerical modelling case study explores simulating the sequential excavation of twin earth pressure balance (EPB) shield tunnels in a representative silty soil profile to analyse ground deformation responses and validate findings against field data. An advanced three-dimensional finite element (FE) modelling to simulate a sequence of tunnel excavations in layered soil profiles containing silts and sands, referencing project geometries, construction methods, and ground parameters as reported in (Chen et al., 2011) . Tunnel segments were modelled with both circular and non-circular cross-sections.

In this case study, a detailed three-dimensional finite element (FE) model is constructed, following the ground profile shown in Figure 1 to replicate the parallel tunnels excavation below a typical urban area, matching the geometry reported in the source: two tunnels of 6.2 m diameter each, spaced 12 m apart, with a tunnel depth of about 19 m in interbedded silty strata. The domain size for the FE model would be selected wide enough (e.g., ≥ 5 tunnel diameters from the tunnel centerline on each side, and about 3 diameters below) to

minimize boundary effects and capture the full extent of settlement troughs and lateral soil movements.

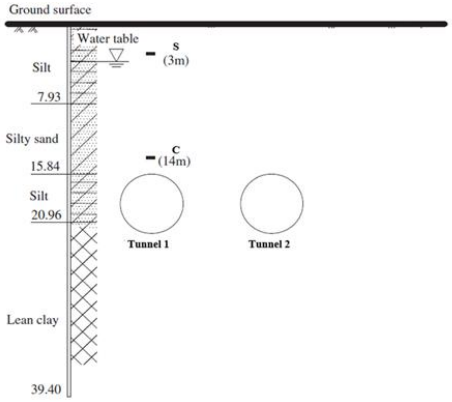

Figure 1. Ground profile along with the tunnel location, after Chen et al. (2011).

Sequential tunnel excavation is simulated in phases (shown in Figure 2): the first (usually left) tunnel is excavated with volume loss controlled by artificially reducing soil properties and implementing a specified percentage of ground loss (typically 0.5–1.5% of tunnel volume, based on observed field behavior). Shield pressure at the face and grouting behind the lining are both simulated to reflect realistic construction procedures and minimize excessive settlement or loss of support.

After significant consolidation around the first tunnel, the second parallel tunnel is advanced with the same methodology. This process enables the model to capture the effect of prior ground improvement (from grouting and soil densification around the initial tunnel) on the performance and ground response during the second drive. Monitoring points, representing real-world settlement markers and extensometers, are integrated into the model above and between the tunnels to record both vertical and horizontal displacements as each stage progresses in the field.

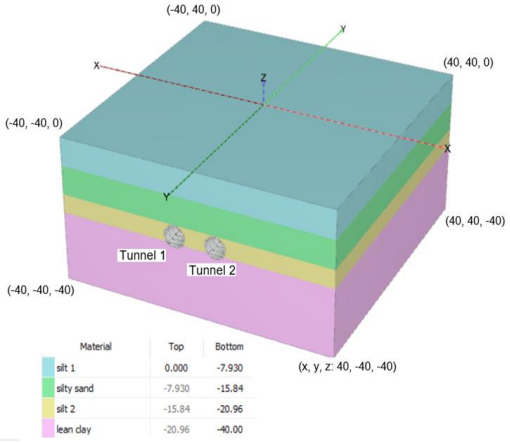

Figure 2. Validation model in PLAXIS 3D.

Simulation outcomes show that most settlements occur as the tunnel face passes beneath monitoring sections, with the maximum surface and subsurface settlements typically observed above the tunnel crown and sometimes enhanced in the central zone between the tunnels. The model demonstrates that pore water pressure fluctuates in response to excavation and grouting; for the second tunnel, modified soil stiffness and reduced permeability from prior grouting are incorporated, leading to characteristically higher pore pressure responses and somewhat reduced settlements compared to the first drive, consistent with field observations.

2.2 *Model Validation*

The horizontal soil displacement in the field derived from the FE simulation reveals initial upward soil movement (heave) as the shield face approaches, then settlement as the face passes and consolidation develops behind the tail. The soil near the invert is shown to move outward under the shield thrust, while the surface soils above gradually converge due to ground loss, mirroring the transition and time-dependent consolidation stages seen in monitored data.

Model results are validated by comparing computed settlements, pore pressures, and lateral displacements with the field measurements reported in the original paper, showing close agreement in both magnitude and trough shape, and reproducing the observed staged response as the second tunnel is driven.

The validation aims to establish the reliability of numerical analyses in predicting tunnel deformations and subsurface levels. Key focus points include locations 3 meters below ground level (Point S) and 14 meters below ground level (Point C, situated just above the crown of the tunnel).

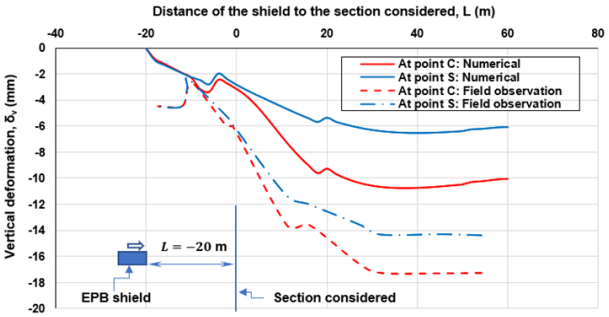

Figure 3. Subsurface settlement profile: Field observation v/s numerical study.

The deformation comparison chart in Figure 3 shows the concurrence between numerical analyses and field measurements. The two distinct curves, representing field deformations and numerical predictions, exhibit a remarkably close alignment. At the critical depth of 3 meters below ground level, both curves trace almost identical paths, signifying a robust agreement between the observed and simulated deformations. A similar pattern is observed at 14 meters below ground level, emphasizing the consistent accuracy of the numerical model in capturing the dynamic behavior of the tunnel structure and surrounding ground.

As the shield nears the considered section (L ≈ -20m to 0), both deep and shallow points first experience slight heave, followed by sharp increase in downward settlement as the face passes beneath. The early upward movements (heave) are more subtle and visible in field data, capturing the initial stress redistribution and the temporary upward pressure imparted by shield excavation. Maximum settlements occur with a lag after the shield has passed, matching both field and simulation trends. The deepest point (C, tunnel crown) shows the greatest maximum settlement. In contrast, the upper, shallower point (S) stabilizes at a lower deformation, confirming surface settlement attenuation with height above the tunnel.

2.3 *Arching Morphology*

The validation findings connect complex modelling to both empirical observation and analytical theory. Taking the study further ahead, the mechanisms of soil arching mobilization and its morphological characteristics are analyzed with an integration into the conventional subsurface settlement studies, which often do not consider the soil arching effects. Two cases were considered as a part of this study where Case A considers

the effects of foundation loading after the tunnel construction, and Case B considers the effects of foundation loading prior to the complete construction of the tunnel. In both cases, tunnel construction was simulated using 9 rings of 2 m each completed by a 0.25 m-thick concrete lining.

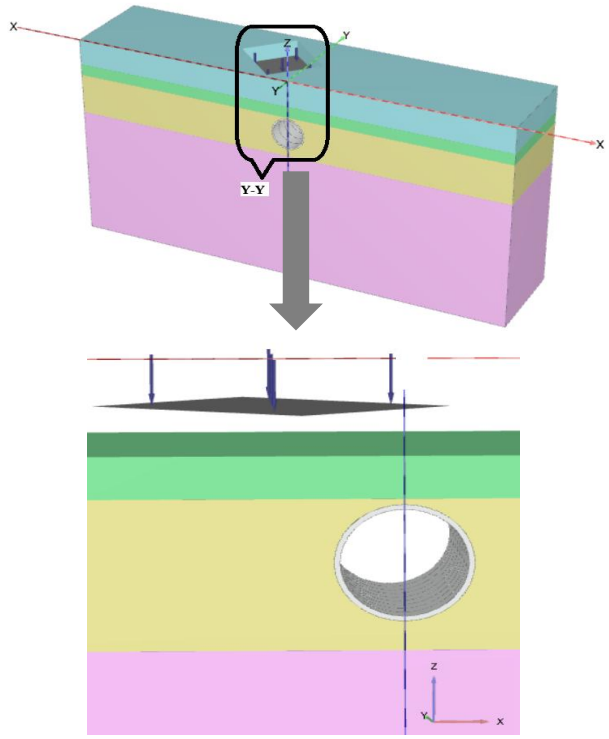

Figure 4. Case A: Input model.

The isometric overview of the complete 3D FE modeling domain, showing the overburden loads redirected laterally as the tunnel is excavated, is shown in Figure 4. The material properties for the model include:

Table 1. Material properties, after Chen et al. (2011).

Parameter	Silt 1	Silty Sand	Silt 2	Dense Sand
Soil model	Hardening Soil	Hardening Soil		
γ_{unsat} (kN/m^3)	19.60	19.70	19	18.10
γ_{sat} (kN/m^3)	20.18	20.63	19.48	19.16
E_{50}^{ref} (kN/m^2)	15x10^3	22x10^3	18x10^3	35x10^3
E_{oed}^{ref} (kN/m^2)	15x10^3	22x10^3	18x10^3	35x10^3
E_{ur}^{ref} (kN/m^2)	35x10^3	60x10^3	40x10^3	75x10^3
ν_{ur}	0.20	0.20	0.20	0.20
c'$_{ref}$ (kN/m^2)	7.9	7.10	9	2
φ' (˚)	30.4	31.40	30.3	27

3 RESULTS AND DISCUSSIONS

The vertical deformation profile for Case A, in Figure 5 illustrates a distinct and concentrated settlement pattern. As tunneling progresses through its various phases, the soil at the surface above the tunnel crown undergoes an increasingly pronounced subsidence. By the final stages, the settlement curve is narrow and deep, with a maximum deformation of nearly -15 mm, focused directly above the tunnel. This narrow and steep trough signals a rapid and efficient mobilization of the soil arch, where vertical loads are quickly transferred laterally due to the rigidity of the tunnel lining or the higher strength and friction angle of the surrounding ground. The steep settlement curve demonstrates that stress redistribution is highly focused, leading to a sharply defined morphological arch feature in the overlying strata resulting from well-developed soil arching.

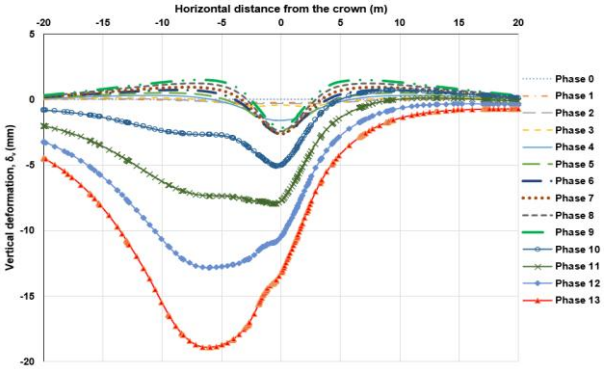

Figure 5. Case A: Deformation in different phases of tunneling.

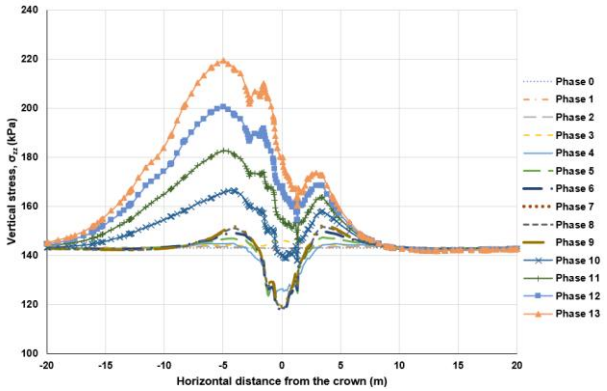

Figure 6. Case A: Stresses in different phases of tunneling.

In contrast, the vertical deformation profile for Case B in Figure 7 presents a broader, more distributed settlement pattern over the tunnel. Early phases reveal a steep drop in surface level, but rather than deepening, the settlement curve rebounds and then stabilizes at a lower level, resulting in a much flatter and wider trough. Maximum settlement occurs earlier and is less pronounced as the curve broadens, indicating that the soil's response is more adaptive and arching is less efficiently mobilized. The diffuse nature of this settlement suggests that the tunnel has a more flexible lining, the soil is less stiff, or inherent ground properties allow for a slower, wider distribution of movement. Consequently, the affected zone encompassing surface settlement widens compared to Case A, and the arch morphology above the tunnel is less sharply defined.

The vertical stress profile for Case A (Figure 6) complements the deformation findings, exhibiting a dramatic reduction in vertical stress just above the tunnel crown, especially in the advanced phases of excavation. The stress 'dip' is steep and local, flanked by abrupt peaks where the arch transfers load into adjacent ground. This narrow, deep reduction in stress is the direct signature of concentrated arching, where the formation of a strong arch above the tunnel effectively 'shields' the crown from overburden loads, rapidly redirecting force to the sides. The local increase in stress beyond the tunnel suggests that the stress pathways created by the arch are efficient, and the soil mobilizes its full frictional and structural potential.

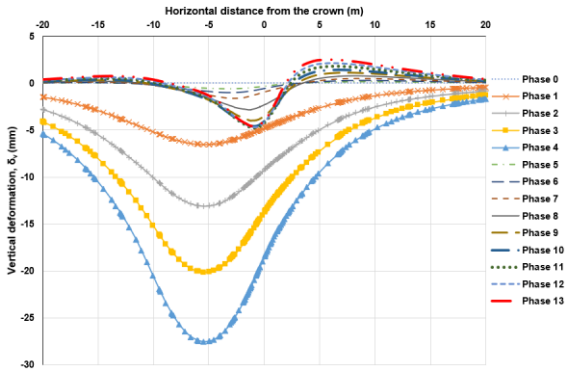

Figure 7. Case B: Deformation in different phases of tunneling.

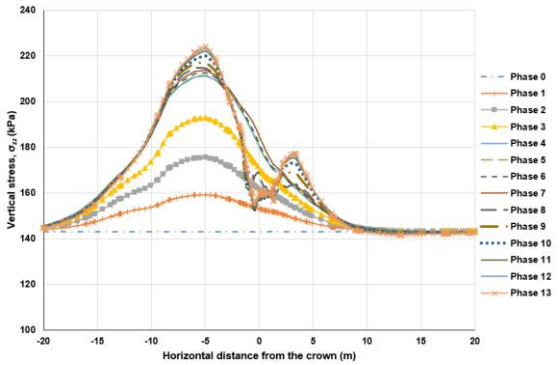

Figure 8. Case B: Stresses in different phases of tunneling.

The vertical stress image for Case B shows a more gradual and distributed shift in stress in Figure 8. Instead of a sharp dip at the crown, the vertical stress increases more broadly above the tunnel during most phases, peaking higher, then gently tapering back to baseline values. The stress transfer zone is not as focused, with the stress dip and rebound covering a significantly larger expanse. This more widespread redistribution reveals that the soil arch formed is flatter and less forceful, a result attributed to greater tunnel flexibility, weaker soils, or less pronounced geometric constraints. The arching effect exists but is mobilized over a broader region, resulting in more gradual changes in stress and a wider affected ground zone.

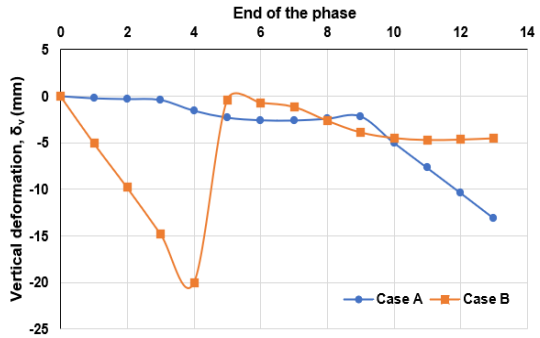

Figure 9. Vertical deformation comparison for Cases A & B.

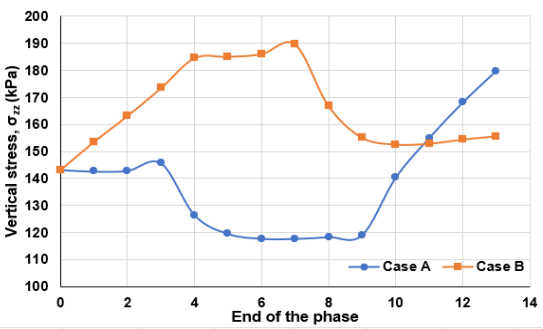

Figure 10. Vertical stress comparison for Cases A & B.

Table 2. Comparison: Case A and Case B

Feature/Aspect	Case A	Case B
Arch Formation	Steep, localized, sharply defined arching above the tunnel	Broader, flatter, more diffuse arching
Settlement Profile	Concentrated settlement with a higher peak directly above the tunnel crown; narrower affected zone	Wider but lower settlement troughs; surface deformation spread across a broader area
Vertical Stress at Crown	Distinctly reduced vertical stress at the tunnel crown	More gradual redistribution; less pronounced reduction at the crown
Deformation Distribution	Surface and subsurface deformations remain focused, higher maximum but within a smaller region	Deformation extends over a much broader zone, but peak settlement is less pronounced

4 CONCLUSIONS

In summary, the high agreement between numerical and field results confirms that the finite element model robustly captures the morphological influence of tunnel stiffness and ground properties on soil arching, settlement, and stress transfer. Recognizing the distinct responses of Cases A and B is essential for effective tunnel design and risk management in varied geological settings.

- Case A: Concentrated arching and focused, higher settlements— for limiting the breadth of ground impact.
- Case B: Diffuse arching, spreading settlement over a wider area with lower peaks—suited for reducing maximum subsidence.
- Understanding these mechanisms enables targeted design, minimized ground risk, and more efficient tunneling solutions.

5 REFERENCES

Chen, R.P., Song, X., Meng, F.Y., Wu, H.N. and Lin, X.T., 2022. Analytical approach to predict tunneling-induced subsurface settlement in sand considering soil arching effect. *Computers and Geotechnics*, 141. https://doi.org/10.1016/j.compgeo.2021.104492.

Chen, R.P., Zhu, J., Liu, W. and Tang, X.W., 2011. Ground movement induced by parallel EPB tunnels in silty soils. *Tunnelling and Underground Space Technology*, 26(1), pp.163–171. https://doi.org/10.1016/j.tust.2010.09.004.

Franza, A., Marshall, A.M. and Zhou, B., 2019. Greenfield tunnelling in sands: The effects of soil density and relative depth. *Geotechnique*, 69(4), pp.297–307. https://doi.org/10.1680/jgeot.17.P.091.

Karl Terzaghi, 1943. *Theoretical soil mechanics*. John Wiley and Sons.

Khandouzi, G. and Khosravi, M.H., 2023. An analytical investigation of soil arching induced by tunneling in sandy ground. *Tunnelling and Underground Space Technology*, 140. https://doi.org/10.1016/j.tust.2023.105242.

Lin, X.T., Chen, R.P., Wu, H.N. and Cheng, H.Z., 2019. Three-dimensional stress-transfer mechanism and soil arching evolution induced by shield tunneling in sandy ground. *Tunnelling and Underground Space Technology*, 93. https://doi.org/10.1016/j.tust.2019.103104.

N. Loganathan and H. G. Poulos, 1998. Analytical prediction for tunneling-induced ground movements in clays.

Song, X., Wu, H.-N., Meng, F.-Y., Chen, R.-P. and Cheng, H.-Z., 2023. Soil arching evolution caused by shield tunneling in deep saturated ground. *Transportation Geotechnics*, [online] 40, p.100966. https://doi.org/https://doi.org/10.1016/j.trgeo.2023.100966.